Experimental Measurement and Numerical Analysis on Resonant Characteristics of Piezoelectric Disks with Partial Electrode Designs

Yu-Chih Lin and Chien-Ching Ma

***Abstract*—Three experimental techniques are used in this study to access the influence of the electrode arrangement on the resonant characteristics of piezoceramic disks. These methods, including the amplitude-fluctuation electronic speckle pattern interferometry (AF-ESPI), laser Doppler vibrometer-dynamic signal analyzer (LDV-DSA), and impedance analysis, are based on the measurement of full-field displacement, pointwise displacement, and electric impedance, respectively. In this study, one full electrode design and three nonsymmetrical partial electrode designs of piezoelectric disks are investigated. Because the clear fringe patterns measured by the AF-ESPI method will be shown only at resonant frequencies, both the resonant frequencies and the corresponding vibration mode shapes are successfully obtained at the same time for out-of-plane and in-plane motions. The second experimental method is the impedance analysis, which is used to measure the resonant and antiresonant frequencies. In addition to these experimental methods, LDV-DSA is used to determine the resonant frequencies of the vibration mode with out-of-plane motion. From the experimental results, the dependence of electrode design on the vibration frequencies and mode shapes is addressed. Numerical computations based on the finite element method are presented, and the results are compared with the experimental measurements. The effect of different designs of electrode is more significant in the in-plane modes than that in the out-of-plane modes.**

I. Introduction

The basic feature of a piezoelectric medium is the piezoelectricity that describes the phenomenon in which the material generates electric charge when subjected to stress and, conversely, generates strain when the electric field is applied. The application of the piezoelectric effect has gradually extended to many modern engineering fields because it connects the communication of the electric field with the mechanical field. Among the various piezoelectric materials, the piezoelectric ceramics, especially of lead zirconate titanate (PZT), is the most preferred type because of its improved properties, such as the inherently high electromechanical transformation efficiency, the piezoelectric activity, and the simplicity to machine into a wide variety of shapes and sizes according to the applications demanded. Recently, the application of piezoceramics was carried out in many research areas, such as high-power ultrasonics transducers [1], sensors and actuators [2], acoustic transmitters in signal processing elements and filter. In most of the applications mentioned above, the disk type specimens are widely used because of their simple geometry that makes them easy to be analyzed. Such applications in piezoelectricity use the resonant characteristics, hence numerous researches have been conducted to study the vibration response of piezoelectric circular disks with electroded faces by the numerical, theoretical, and experimental methods. Among these methods, the theoretical analysis is restricted to certain boundaries and very simple geometry, and the numerical computation and experimental measurement usually are used to study the vibration characteristics of piezoelectric devices. Kharouf and Heyliger [3] used the Rayleigh-Ritz method to solve the static and axisymmetrical vibration problems for piezoelectric disks, hollow cylinders, and composite cylinders. Kunkel *et al.* [4] studied the vibration modes of PZT-5H ceramics disks for the diameter-to-thickness (D/T) ratio ranging from 0.2 to 10. Guo *et al.* [5] presented the results for PZT-5A piezoelectric disks with D/T of 20 and 10. Five types of modes were classified according to the mode shape characteristics, and the physical interpretation was well clarified. Shaw [6] used an optical interference technique to measure the surface motion of thick barium titanate disks. Schmidt [7] computed the first resonance frequency of a circular plate as a function of the radius of the electrodes and compared it with the measured values. Bogy and coworkers [8], [9] used an approximate two-dimensional theory to predict the output voltage generated in circular PZT disks after a sudden release from a static deformation caused by axisymmetric and nonaxisymmetric loads. Huang and Ma [10] investigated the full-field vibration amplitude distribution of piezoceramic disks with fully covered electrode by AF-ESPI and impedance techniques. Ivina [11] used the finite-element method to analyze the thickness-symmetrical vibrations of circular piezoelectric plates with two different partial electrodes. Ohno [12] established the calculation method for resonance modes of piezoelectric crystals, and Ogi *et al.* [13] computed and measured the resonance frequencies of

Manuscript received October 9, 2003; accepted February 5, 2004. The authors gratefully acknowledge the financial support of this research by the National Science Council (Republic of China) under Grant NSC 91-2212-E-002-058.

The authors are with the Department of Mechanical Engineering, National Taiwan University, Taipei, Taiwan 10617, Republic of China (e-mail: ccma@ntu.edu.tw).

lithium niobate. However, few studies have been published on the analysis of the resonant characteristics in PZT disks with partially covered nonaxisymmetrical electrodes experimentally, especially for the full-field measurement of mode shapes. In this study, three experimental techniques and the finite-element analysis are used to investigate the vibration of piezoceramic disks with four electrode designs. Both in-plane and out-of-plane vibrations of the PZT disks are studied in detail.

The first experimental technique that provides the full-field deformation of the vibrating piezoelectric disks in resonance is the electronic speckle pattern interferometry (ESPI), which is also known as TV-holography. It was first proposed by Butters and Leendertz [14] and was improved by numerous researchers [15]–[18] to become an advanced technique for vibration mode analysis. The most convenient experimental setup of vibration measurement by ESPI is the time-averaging method that yields a video image of a vibrating object with correlation fringes superimposed. However, the restrictions of the time-averaging method are decreased visibility with vibration amplitude, and limited numbers of fringes. Wang *et al.* [19] proposed the amplitude-fluctuation ESPI (AF-ESPI) technique based on video-signal-subtraction, but the reference image was taken from a vibrating state instead of a free state. The fringe patterns obtained by the AF-ESPI method have enhanced visibility and reduced noise. Huang and Ma [20] and Ma and Huang [21] further applied the AF-ESPI to investigate three-dimensional volume vibrations of piezoelectric materials. In their works, the interferometric fringe patterns obtained by AF-ESPI were clearly displayed with high quality for identification of resonant frequencies and mode shapes.

The second optical measurement technique used in this study is the laser Doppler vibrometer (LDV), which measures the moving velocity or displacement of an object by detecting the frequency shift of the laser. The resonant frequencies of out-of-plane vibration can be obtained because the peaks appearing in the frequency-response curve correspond to resonant frequencies.

The electric impedance is an important characteristic for piezoelectric elements, and the experimental measurement of resonant frequencies for the piezoelectric materials generally is performed by impedance analysis. Hence, the third experimental technique used in this work is the impedance analysis. Because the electric impedance will drop to a local minimum when it vibrates at a resonant frequency and will raise to local maximum at an antiresonant frequency, the resonant and antiresonant frequencies can be determined from the frequency-impedance curve obtained by impedance analysis. In addition of these three experimental techniques, numerical computations based on the finite-element method (FEM) using the commercial software package, ABAQUS (Hibbit, Karlsson, and Sorensen, Inc., Pawtucket, RI) also is made. The resonant frequencies measured by AF-ESPI are compared with those obtained by LDV, impedance analysis, and with those computed by FEM. The corresponding mode shapes obtained by AF-ESPI and calculated by FEM also are presented for comparisons. It is found in this study that the mode shapes and resonant frequencies of the first eight modes for the out-of-plane motion are almost the same for different electrode design. However, the vibration characteristics of the in-plane motion are strongly influenced by the electrode designs.

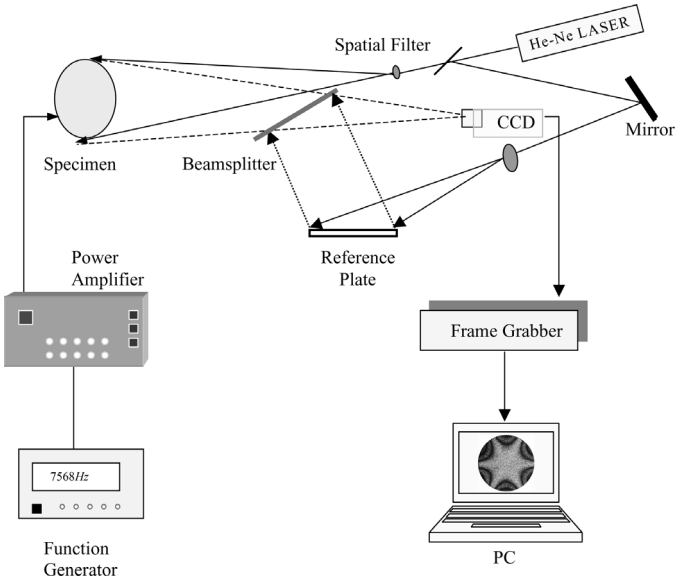

Fig. 1. Schematic of the AF-ESPI setup for out-of-plane measurement.

II. Theory of AF-ESPI Technique

The AF-ESPI setup and theory were described in detail by Ma and Huang [21]. We present them briefly as follows:

A. Out-of-Plane Vibration

The experimental setup of ESPI for out-of-plane measurement is shown in Fig. 1. At a given instant time t, the light intensity in the image plane detected by a charge-coupled device (CCD) camera (Pulnix TM-7CN, Pulnix America, Inc., Sunnyvale, CA) can be expressed as:

$$I(t) = I_R + I_O + 2\sqrt{I_R I_O}\cos\left[\phi + \frac{2\pi}{\lambda}(1+\cos\theta)A(t)\right], \quad (1)$$

where I_R = the reference light intensity, I_O = the object light intensity, ϕ = the phase difference between reference and object light, λ = the wavelength of laser, θ = the angle between object light and observation direction, and $A(t)$ = the amplitude of a given point on the object.

The light intensity averaged over the CCD refreshing time τ by using the time-averaged method is:

$$I_\tau = I_R + I_O + \frac{2\sqrt{I_R I_O}}{\tau}\int_0^\tau \cos\left[\phi + \frac{2\pi}{\lambda}(1+\cos\theta)A(t)\right]dt. \quad (2)$$

Assume the specimen vibrates periodically, the intensity average I_τ can be written as:

$$I_\tau = I_R + I_O + \frac{2\sqrt{I_R I_O}}{\tau}\int_0^\tau \cos(\phi + \Gamma A\cos\omega t)dt$$
$$= I_R + I_O + \frac{2\sqrt{I_R I_O}}{\tau}\mathrm{Re}\left\{e^{i\phi}\int_0^\tau \exp(i\Gamma A\cos\omega t)dt\right\},$$

where Re stands for the real part, $A(t) = A\cos\omega t$ and ω is the angular frequency. $\Gamma = \frac{2\pi}{\lambda}(1+\cos\theta)$ and $\tau = \frac{2m\pi}{\omega}$, where m is an integer. The intensity of the first image, named as the reference image, can be expressed as:

$$I_\tau = I_R + I_O + 2\sqrt{I_R I_O}|(\cos\phi)J_0(\Gamma A)|, \quad (3)$$

where J_0 is a zeroth order Bessel function of the first kind. As the vibration of the specimen continues, we can assume that the vibration amplitude changes from A to $A + \Delta A$ because of the electronic noise or instability of the apparatus, then the light intensity of the second image I'_τ can be represented as:

$$I'_\tau = I_R + I_O + 2\sqrt{I_R I_O}\left|(\cos\phi)\left[1 - \frac{1}{4}\Gamma^2(\Delta A)^2\right]J_0(\Gamma A)\right|. \quad (4)$$

When these two images (the reference and second images) are subtracted by the image processing system, i.e., (3) is subtracted from (4), and are rectified, the resulting image intensity can be expressed as:

$$I = I'_\tau - I_\tau = \frac{\sqrt{I_R I_O}}{2}\left|(\cos\phi)\Gamma^2(\Delta A)^2 J_0(\Gamma A)\right|. \quad (5)$$

B. In-Plane Vibration

The experimental setup of the AF-ESPI system for in-plane vibration measurement is shown in Fig. 2. Similar to the out-of-plane vibration measurement, the reference and second image intensities, i.e., I_τ and I'_τ for in-plane vibration are expressed as:

$$I_\tau = 2I_O + 2I_O\left|(\cos\phi)J_0(\Gamma' A')\right|, \quad (6)$$

and

$$I'_\tau = 2I_O + 2I_O\left|(\cos\phi)\left[1 - \frac{1}{4}\Gamma'^2(\Delta A')^2\right]J_0(\Gamma' A')\right|, \quad (7)$$

where I_O = the object light intensity, A' = the vibration amplitude of in-plane vibration, $\Gamma' = \frac{2\pi}{\lambda}(2\sin\theta')$ and θ' = half of the angle between two object lights.

Subtracting (6) from (7) and rectifying by the image processing system, we can obtain the resulting image intensity as:

$$I = I'_\tau - I_\tau = \frac{I_O}{2}\left|(\cos\phi)\Gamma'^2(\Delta A')^2 J_0(\Gamma' A')\right|. \quad (8)$$

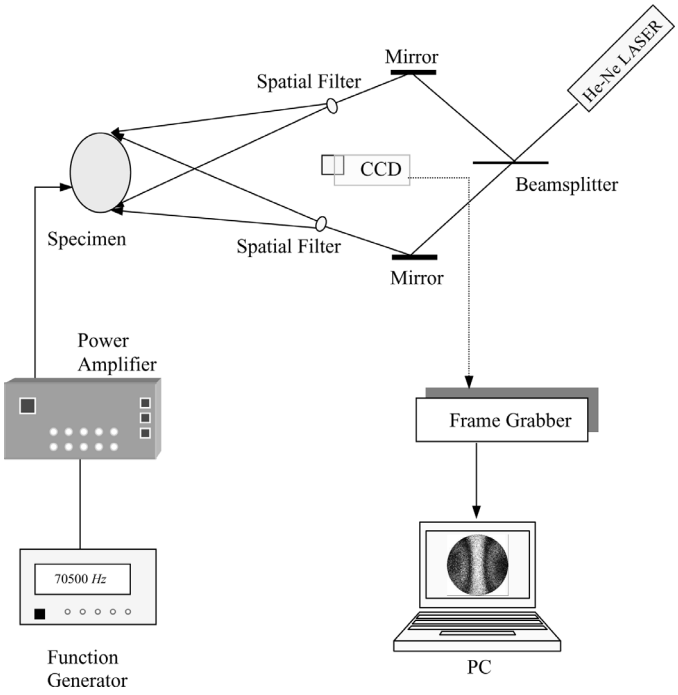

Fig. 2. Schematic of the AF-ESPI setup for in-plane measurement.

Combining the out-of-plane with in-plane optical setups by the AF-ESPI method, we can study completely the vibration characteristics of the piezoceramic material, including resonant frequencies and mode shapes at the same time.

III. Specimens and Experimental Setup

The vibration characteristics of traction-free piezoceramic disks with diametric cuts on electroded plane faces are investigated in this section. The thickness-polarized piezoceramic disk with a diameter of 30 mm and a thickness of 1 mm is made of $Pb(Zr\cdot Ti)O_3$ ceramics; its model number is PIC-151 (Physik Instrumente, Lederhose, Germany). The material properties of this piezoceramic disk used for numerical computation are listed in Table I. The material properties were provided by Physik Instrumente. Analytically, boundary conditions can be specified as completely free or any constrained situations. The completely free boundary means that the specimen is, in fact, floating in space with no attachment or connection in ground and exhibits rigid body behavior at zero frequency. In testing practice, however, it is almost not realizable and generally not possible to fully achieve this condition. Hence, the specimen must be supported in some manner to model the completely free boundary. In this study, to experimentally model the completely free boundary, the piezoceramic disk is placed on the surface of a very soft sponge with the dimensions $80\times60\times23$ mm and is stuck by a narrow adhesive tape on the surface of the sponge. The optical layout of the AF-ESPI systems, as shown in Figs. 1 and 2, is used to perform the out-of-plane and in-plane measurements for resonant frequencies and corresponding mode shapes.

TABLE I
MATERIAL PROPERTIES OF PIC-151.

Quality	PIC-151
C_{11}^E (N/m^2)	10.76×10^{10}
C_{12}^E	6.313×10^{10}
C_{13}^E	6.386×10^{10}
C_{33}^E	10.04×10^{10}
C_{44}^E	1.962×10^{10}
C_{66}^E	2.224×10^{10}
e_{31} (N/Vm)	-9.52
e_{33}	15.14
e_{15}	11.97
ρ (Kg/m^3)	7800
$\varepsilon_{11}^s/\varepsilon_0$	1111
$\varepsilon_{33}^s/\varepsilon_0$	925
ε_0	8.85×10^{-12}

A He-Ne laser (25-LHP-928-249, Melles Griot, Carlsbad, CA) with 35 mW and wavelength $\lambda = 632.8$ nm is used as the coherent light source. The emitting laser beam is split into two parts by a variable beamsplitter. In out-of-plane layout as shown in Fig. 1, one beam is directed toward the piezoceramic disk, then reflects to the CCD camera acting as the object beam; the other one, which serves as a reference beam, is illuminated on the surface of a reference plate and reflects into the CCD camera via the beamsplitter. The object and reference beams are combined into the CCD sensor array through a zoom lens (Nikon Micro-Nikkor 55 mm, Nikon, Melville, NY). In in-plane layout as shown in Fig. 2, the piezoceramic disk is illuminated by two beams incident at equal and opposite angles θ to the surface normal; the disk surface is viewed in the normal direction by a zoom lens. A CCD camera, and a frame grabber (Dipix P360F, Dipix Technologies Inc., Ottawa, Ontario, Canada) with a digital signal processor on board are used to record and process the images obtained from interferogram of the object and reference beams. Once the specimen vibrates, the interferogram recorded by the CCD camera is stored in an image buffer as a reference image. Then the next frame is grabbed and subtracted by the image processing system. The CCD camera converts the intensity distribution of the interference pattern of the object into a corresponding video signal at 30 frames per second. The signal is electronically processed, then converted into an image on the video monitor. The interpretation of the fringe image is similar to the reading of a displacement contour. Note that the vibration displacements obtained from the experimental system for the AF-ESPI method are in the order of submicrometer. To achieve a sinusoidal output, a digitally controlled function generator (HP-33120A, Hewlett Packard, Palo Alto, CA) connected to a power amplifier (NF Electronic Instruments 4005 type, NF Corporation, Kohokuku, Yokohama, Japan) is used as an input source, which generates a periodical exciting force to the specimen.

Detailed experimental procedure of the AF-ESPI technique for both the in-plane and the out-of-plane vibrations is performed as follows. First, a reference image is taken after the specimen vibrates with the second image taken subsequently; the reference image is subtracted by the image processing system. If the vibrating frequency is not the resonant frequency, only randomly distributed speckles are displayed and no fringe patterns will be shown. In case the vibrating frequency falls in the neighborhood of the resonant frequency, distinct stationary fringe patterns will be observed in the monitor. Then, the function generator is carefully and gradually turned; the number of fringes will increase and the fringe pattern will become clearer as the resonant frequency is approached. From the aforementioned experimental procedure, the resonant frequencies and the correspondent mode shapes can be determined at the same time by using the AF-ESPI optical system.

Second, the experimental optical method, the LDV (AVID, Ahead Optoelectronics Inc., Chung-Ho, Taipei, Taiwan), which is a pointwise displacement measurement technique, also is used to investigate the out-of-plane vibration characteristics of the piezoelectric disk. The focusing lens of the LDV system is 90 mm, and the size of the laser spot is 52 μm. This system has an extremely wide signal bandwidth and an ultra-high resolution that is in the order of nanometers. However, in obtaining the full-field displacements, the LDV system is much more time consuming than the AF-ESPI system. The optical system is based on the principle of Michelson interferometer and the Doppler effect. A built-in dynamic signal analyzer (DSA) is integrated into the LDV system to become the LDV-DSA system. The DSA unit is composed of the analysis software and a plug-in waveform generator board that can provide the swept-sine excitation signal. In the analysis software, the swept-sine excitation signal is taken as input, and the response measured by LDV is converted into the voltage signal and is taken as output. After the fast Fourier transform (FFT) processing of the input and output with the DSA software, the ratio of output/input ("gain") is obtained. The results chart that shows the frequency response curve can be obtained. The peak values appearing in the frequency response curve are the resonant frequencies. A detailed description of the LDV-DSA system and the working principle can be found in [22].

In addition to the experimental measurements, numerical computations of resonant frequencies and mode shapes also are implemented by ABAQUS finite-element package, in which three-dimensional, 20-node solid piezoelectric elements (C3D20RE) are selected to analyze the problem. For the convenience of explanation, the following abbreviated symbols are used for specifying the piezoceramic disk with four electrode arrangements:

Case I. No cut is applied on the faces of disk; the two surfaces of the piezoceramic disk are completely coated by silver electrodes. The schematic diagram illustrating the configuration of the electrode is shown in Fig. 3(a).

Case II. A diametric cut is applied on one of the electroded surfaces; the schematic diagram is shown in Fig. 3(b).

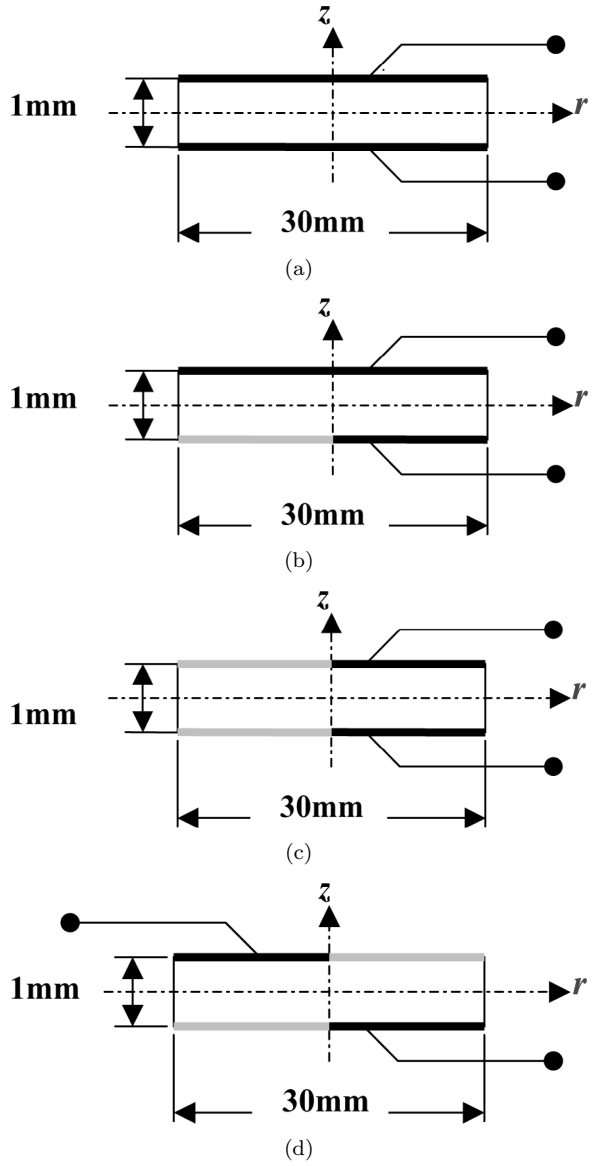

Fig. 3. Schematic of the four electrode designs.

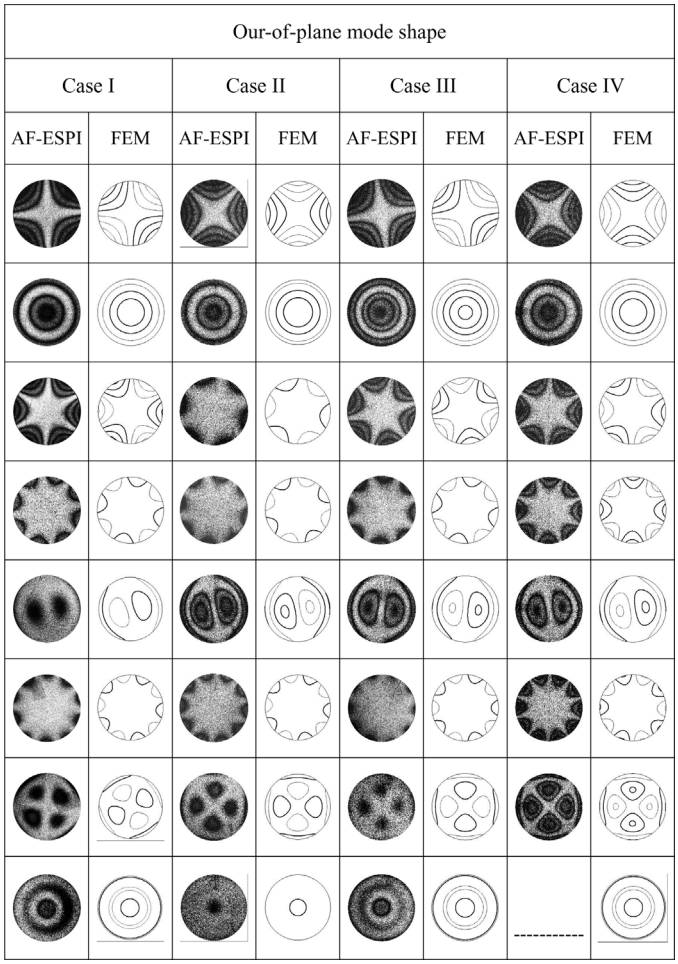

Fig. 4. Mode shapes of out-of-plane modes obtained by AF-ESPI and FEM.

Case III. Both surfaces are cut diametrically, and the electric potential is applied to the same half region of each surface, as shown in Fig. 3(c).

Case IV. The cut is the same as Case III, but the electric potential is applied to the opposite region of each surface. The schematic diagram is shown in Fig. 3(d).

The main reason four types of electrodes are chosen for investigation is that only one piezoceramic specimen is needed in the experimental measurement. As shown in Fig. 3, after finishing the measurement for Case I of full electrode, only one diametric cut in the bottom surface can be used as the specimen for Case II, then another diametric cut in the upper surface is used as the specimen for Cases III and IV. The advantage of using the same piezoceramic disk for different electrode design is that the error of experimental measurement of resonant frequencies induced by using different specimen which may be different slightly in the material properties, and geometric dimensions can be eliminated. Furthermore, these four electrode designs include one symmetric and three quite different unsymmetric problems.

IV. Experimental and Numerical Results

Fig. 4 shows the first eight out-of-plane mode shapes of the PIC-151 piezoceramic disk by using the AF-ESPI and FEM. For the finite element results as shown in Fig. 4, the dashed lines indicate the concave displacements; the solid lines denote convex displacements. The zero-order fringes, which are the brightest fringes on the experimental results, represent the nodal lines of the piezoceramic disk in resonance. The rest of the fringes are contour of constant displacements. It is indicated in Fig. 4 that the out-of-plane mode shape does not change with different electrode design. The fringe patterns of each mode obtained from Case IV electrode design are all clear, except for the eighth mode. In addition to the AF-ESPI method, an alternative experimental technique LDV, which is used to measure the out-of-plane displacement, also is used to identify the resonant frequencies for out-of-plane modes of the piezoceramic disk. The frequency response curves of

TABLE II
RESULTS OF RESONANT FREQUENCIES FOR THE OUT-OF-PLANE VIBRATION FOR PIEZOELECTRIC DISKS WITH FOUR ELECTRODE DESIGNS.[1]

Mode	Method	Case I	Case II	Case III	Case IV
1	AF-ESPI	3230	3245	3230	3240
	LDV (error %)	3310 (2.48)	3210 (−1.08)	3210 (−0.62)	3210 (−0.93)
	FEM (error %)	3192 (−1.18)	3192 (−1.63)	3193 (−1.15)	3192 (−1.48)
2	AF-ESPI	6050	6365	6310	6460
	LDV (error %)	6110 (0.99)	6410 (0.71)	6510 (3.17)	6510 (0.77)
	FEM (error %)	6989 (15.52)	6989 (9.80)	6991 (10.79)	6989 (8.19)
3	AF-ESPI	7568	7543	7545	7600
	LDV (error %)	7610 (0.55)	7610 (0.89)	7610 (0.86)	7610 (0.13)
	FEM (error %)	7492 (−1.00)	7492 (−0.68)	7495 (−0.66)	7492 (−1.42)
4	AF-ESPI	13180	13250	13250	13350
	LDV (error %)	13310 (0.99)	13310 (0.45)	13410 (1.21)	13410 (0.45)
	FEM (error %)	13204 (0.18)	13204 (−0.35)	13215 (−0.26)	13205 (−1.09)
5	AF-ESPI	13574	13913	13945	14140
	LDV (error %)	13710 (1.00)	14010 (0.70)	14210 (1.90)	14210 (0.50)
	FEM (error %)	15094 (11.20)	15094 (8.49)	15100 (8.28)	15094 (6.75)
6	AF-ESPI	20257	20353	20400	20520
	LDV (error %)	20410 (0.76)	20510 (0.77)	20410 (0.05)	20610 (0.44)
	FEM (error %)	20243 (−0.07)	20244 (−0.54)	20272 (−0.63)	20246 (−1.34)
7	AF-ESPI	23060	23520	23475	23840
	LDV (error %)	23410 (1.52)	23810 (1.23)	24110 (2.71)	24110 (1.13)
	FEM (error %)	25157 (9.09)	25158 (6.96)	25184 (7.28)	25160 (5.54)
8	AF-ESPI	25550	25823	25975	—
	LDV (error %)	25610 (0.23)	26210 (1.50)	26510 (2.06)	—
	FEM (error %)	27924 (9.29)	27927 (8.15)	27951 (7.61)	27929

[1]The units of the frequencies are hertz.

piezoceramic disks measured by LDV-DSA are shown in Fig. 5. Fig. 5(b) shows that the eighth mode for partial electrode Case IV is not identified by the LDV either. It is evident from the experimental measurement that the eighth mode for Case IV is difficult to excite in the practical application. Table II tabulates the first eight out-of-plane resonant frequencies obtained by the AF-ESPI, LDV, and FEM methods. These results indicate that the resonant frequencies measured by the two experimental techniques have weak dependence only on different electrode design in out-of-plane motion, but the FEM method predicts almost the same result for four electrode designs. The difference of resonant frequencies measured by AF-ESPI and LDV is less than 3%.

The in-plane mode shapes obtained by AF-ESPI and FEM are shown in Figs. 6–9. The U and V directions indicated in Figs. 6–9 are the displacements of the in-plane motions for piezoceramic plates. The U (or V) direction is perpendicular (or parallel) to the diametric cut of the electroded surface. The resonant frequencies for the in-plane modes measured by the AF-ESPI, impedance, and FEM are listed in Table III. In Figs. 6–9 and Table III, we only present the piezoelectric active modes. The mode numbers indicated in Table III are based on the electrode design for Case III, and we put the similar mode shape for different electrode design in the same mode number. The characteristics of the in-plane modes are completely different from those of the out-of-plane modes. The out-of-plane mode shapes and correspondent resonant frequencies are almost the same for different electrode design. However, the in-plane mode shapes and correspondent resonant frequencies are quite different for the four electrode designs. Only the symmetric modes are excited for the out-of-plane modes, but many unsymmetric modes are observed for the in-plane modes for Cases II and III electrode designs.

Because the electric impedance will drop to a local minimum when it vibrates at a resonant frequency, the resonant frequencies also can be obtained by the impedance analysis. Figs. 10(a) and (b) show the impedance curves of the piezoceramic disk with different electrode designs measured by a HP4194A impedance/gain-phase analyzer (Hewlett Packard, Palo Alto, CA). The local minima and maxima appearing in the impedance curve correspond to the resonance and antiresonance, respectively. It is indicated in Fig. 10 that the resonant frequencies obtained by the impedance analysis are all in-plane modes. Within the frequency range of 450 kHz, there are 4, 10, 16, and 3 resonant frequencies identified from impedance curves for the electrode design of Cases I, II, III, and IV, respectively. There are some nonpiezoelectric active modes also shown in the impedance curves for Cases II and III. The results of resonant frequencies for piezoelectric active modes also are shown in Table III, and the correspondent mode shapes are presented in Figs. 6–9.

Because the electrode design for Case I is full electrode, hence the four mode shapes presented in Fig. 6 are symmetric modes. This is evident from Fig. 6 that the mode shapes for U and V displacements are the same. This case has undergone much more intensive study than the others. The fourth mode presented in Fig. 6 is very difficult to excite and it corresponds only to a small variation of the impedance curve in Fig. 10(a). Because of the asymme-

TABLE III
RESULTS OF RESONANT FREQUENCIES FOR THE IN-PLANE VIBRATION FOR PIEZOELECTRIC DISKS WITH FOUR ELECTRODE DESIGNS.[1]

Mode	Method	Case I	Case II	Case III	Case IV
1	AF-ESPI	—	51600	51440	—
	Impedance	—	51788	51339	—
	(error %)		(0.36)	(−0.20)	
	FEM	—	50446	50450	—
	(error %)		(−2.24)	−1.92)	
2	AF-ESPI	70500	72160	72000	76200
	Impedance	70484	72684	72586	76335
	(error %)	(−0.02)	(0.73)	(0.81)	(0.18)
	FEM	64368	71547	71872	82299
	(error %)	(−8.70)	(−0.85)	(−0.18)	(8.00)
3	AF-ESPI	—	119940	117600	—
	Impedance	—	119973	117577	—
	(error %)		(0.03)	−0.02)	
	FEM	—	116505	116569	—
	(error %)		(−2.86)	(−0.88)	
4	AF-ESPI	—	130960	130130	—
	Impedance	—	130970	130074	—
	(error %)		(0.01)	(−0.04)	
	FEM	—	129815	130063	—
	(error %)		(−0.87)	(−0.05)	
5	AF-ESPI	180279	184500	183800	183760
	Impedance	182659	184858	183813	183813
	(error %)	(1.32)	(0.19)	(0.01)	(0.03)
	FEM	167404	180292	181142	201166
	(error %)	(−7.14)	(−2.28)	(−1.45)	(9.47)
6	AF-ESPI	—	211220	210050	—
	Impedance	—	211252	210058	—
	(error %)		(0.02)	(0.00)	
	FEM	—	212300	212859	—
	(error %)		(0.51)	(1.34)	
7	AF-ESPI	—	236540	232560	—
	Impedance	—	236546	232554	—
	(error %)		(0.00)	(0.00)	
	FEM	—	233834	234312	—
	(error %)		(−1.14)	(0.75)	
8	AF-ESPI	288900	292600	288700	288150
	Impedance	290434	292634	287543	288792
	(error %)	(0.53)	(0.01)	(−0.40)	(0.22)
	FEM	265147	285929	287628	314036
	(error %)	(−8.22)	(−2.28)	(−0.37)	(8.98)
9	AF-ESPI	—	342100	337470	—
	Impedance	—	342122	337533	—
	(error %)		(0.01)	(0.02)	
	FEM	—	340801	344220	—
	(error %)		(−0.38)	(2.00)	
10	AF-ESPI	390400	—	391200	—
	Impedance	393811	—	390022	—
	(error %)	(0.87)		(−0.30)	
	FEM	360988	—	394455	—
	(error %)	(−7.53)		(0.83)	

[1]The units of the frequencies are hertz.

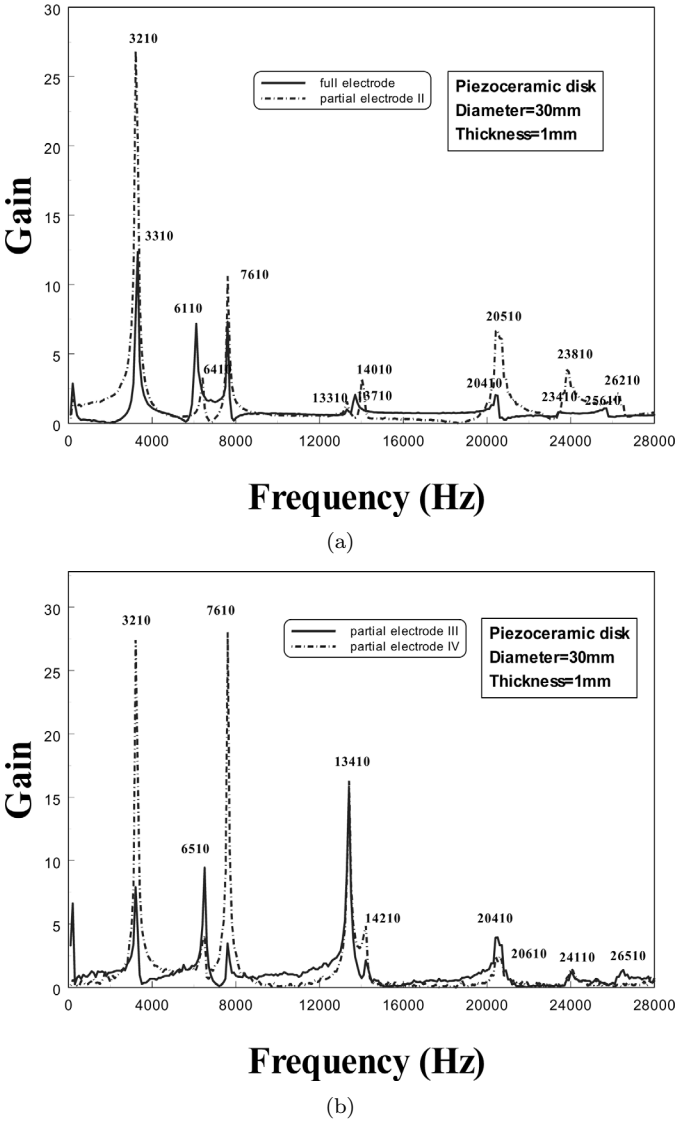

(a)

(b)

Fig. 5. (a) LDV output gain spectrum of transverse vibrations for the piezoceramic disks with full-electrode and partial electrode Case II. (b) LDV output gain spectrum of transverse vibrations for the piezoceramic disks with partial electrode Cases III and IV.

try of electrodes, the mode shapes of Cases II and III are asymmetry and with different displacements in the U and V directions. It is also shown from Figs. 10(a) and (b) that many local minima are indicated in the impedance curve. We note that only three in-plane modes can be excited for the special electrode design of Case IV as presented in Figs. 9 and 10(b). However, 17 out-of-plane modes can be excited easily for Case IV. Hence, it is concluded that the electrode design has a strong influence on the vibration characteristics of piezoceramic disks in resonance.

The differences of resonant frequencies obtained from the ESPI measurements and impedance analysis and that between ESPI results and finite-element computations are indicated in Table III. The differences between the AF-ESPI and impedance are less than 1% in general, and those between the AF-ESPI and FEM are less than 9%. This suggests that the resonant frequencies obtained by AF-

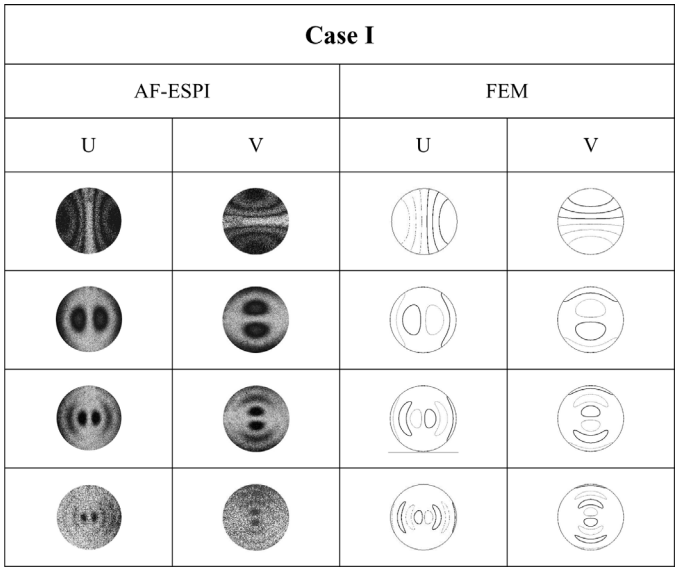

Fig. 6. In-plane mode shapes for Case I obtained by AF-ESPI and FEM.

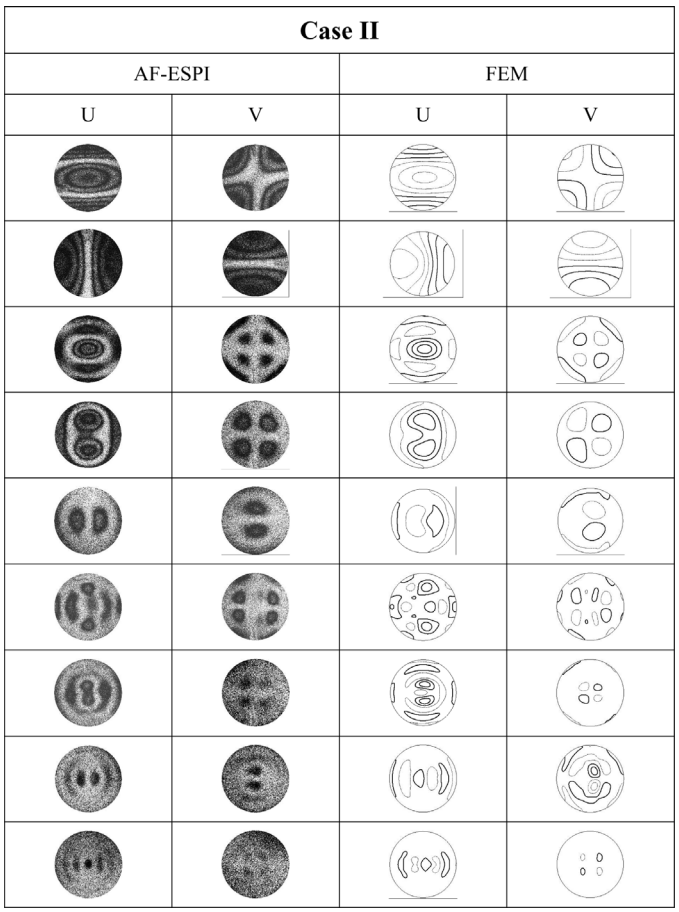

Fig. 7. In-plane mode shapes for Case II obtained by AF-ESPI and FEM.

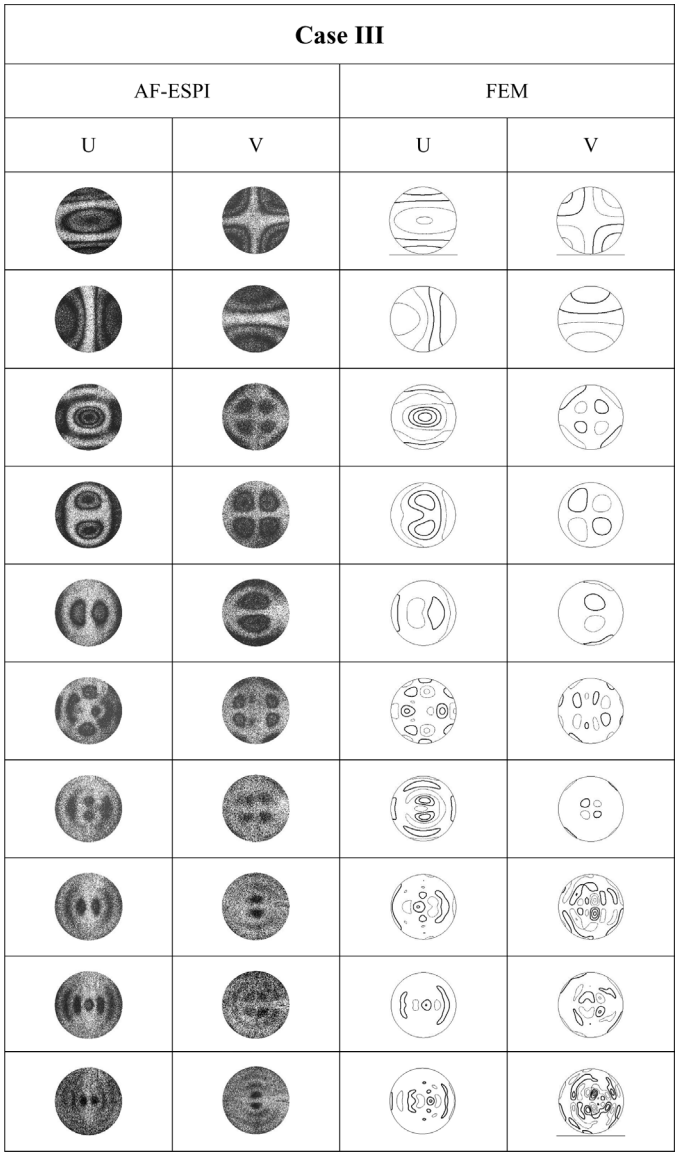

Fig. 8. In-plane mode shapes for Case III obtained by AF-ESPI and FEM.

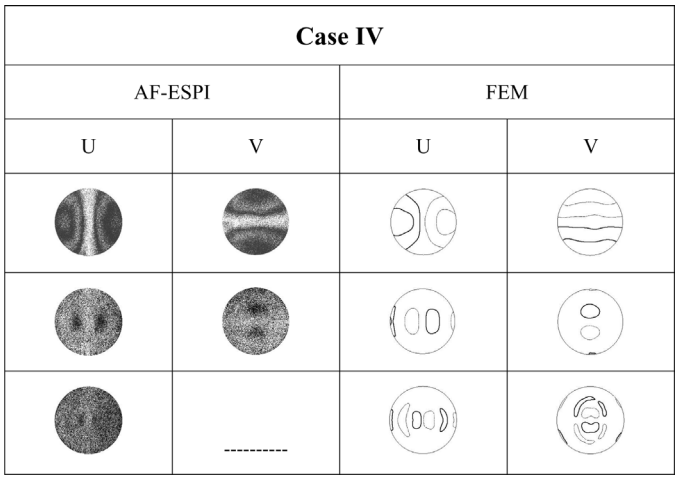

Fig. 9. In-plane mode shapes for Case IV obtained by AF-ESPI and FEM.

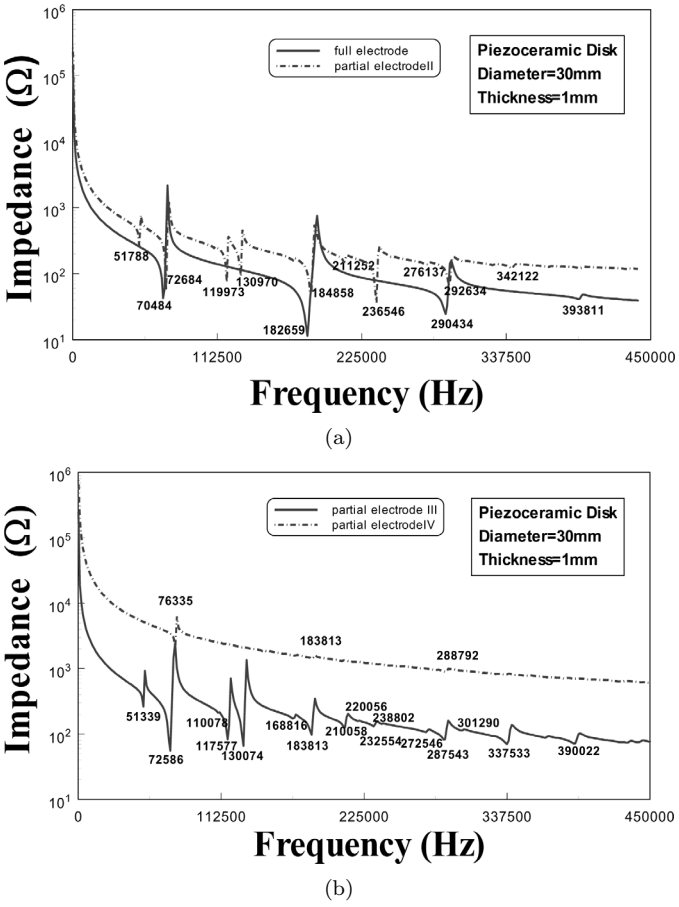

Fig. 10. (a) Impedance variation curve of the piezoceramic disks with full electrode and partial electrode Case II. (b) Impedance variation curve of the piezoceramic disks with partial electrode Cases III and IV.

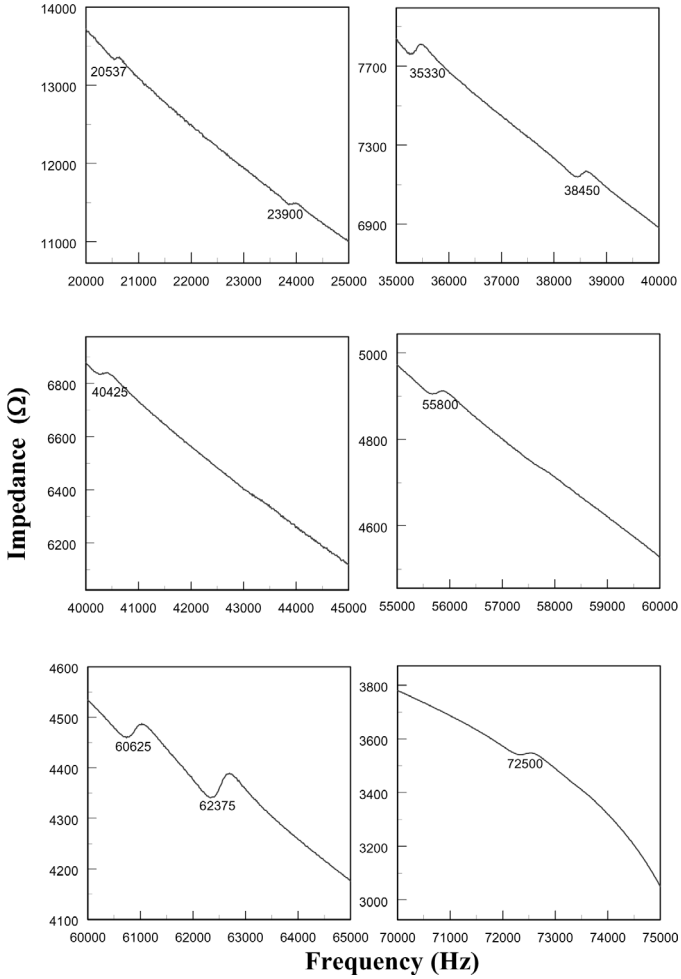

Fig. 11. Impedance variation curve of the piezoceramic disk with Case IV electrode design in 0–75 kHz.

ESPI are in good agreement with the impedance analysis, but there is a slight difference compared with the FEM results, especially in Cases I and IV. It is noted that the FEM calculation for vibration analysis usually gets more inaccurate as the frequency becomes higher.

To get further information, we measured in detail the impedance in low frequencies (below those of the first modes shown in Table III). It was theoretically proved by Huang *et al.* [23] that the impedance of the piezoceramic disk will not have variations at the resonant frequencies for the out-of-plane modes. However, large variations are predicted by the theoretical analysis for the in-plane radial modes. In this study, only smooth decaying curves are observed in experiments for Cases I, II, and III, except Case IV. There are many small variations in the impedance curve shown in Fig. 11 that cannot be found if the scale is not exaggerated in the low frequencies of Case IV. It is interesting to note that the local minima presented in Fig. 11 corresponds to the resonant frequencies for the out-of-plane modes. Table IV shows the LDV, impedance analysis, ESPI, and FEM results in 0–75 kHz. The higher modes can be excited easily only for the special electrode design of Case IV. Table IV also indicates that not every out-of-plane mode can be identified from the impedance curve shown in Fig. 11. Only nine resonant frequencies for the out-of-plane modes are clearly shown in Fig. 11, and they are compared very well with the results obtained from ESPI and LDV. These nine out-of-plane modes can be identified from the impedance curve because the induced magnitude of the in-plane motion by these out-of-plane modes is large and result in the appearance of the local minima in the impedance curve.

V. Conclusions

Because the mechanical and electric fields are coupled in piezoelectric materials, the energy transformation between the electrical and mechanical energy in piezoceramic disks varies with different electrode design. This results in the influence of electrode design on the vibration modes and the resonant frequencies of the piezoceramic disk. In this study, the vibration characteristics for four different electrode designs of a piezoceramic disk were investigated in detail by theoretical calculations and experimental measurements. The results of one full electrode design and three nonsymmetrical partial electrode designs are pre-

TABLE IV
RESULTS OF RESONANT FREQUENCIES AND MODE SHAPES OF CASE IV ELECTRODE DESIGN IN 0–75 KHZ.[1]

LDV	Impedance analyzer	ESPI mode shape (frequency)	FEM mode shape (frequency)
3210	—	 (3240)	 (3192)
6410	—	 (6460)	 (6989)
7610	—	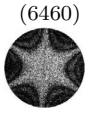 (7600)	 (7492)
13610	—	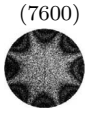 (13350)	 (13205)
14410	—	 (14140)	 (15094)
20410	20537	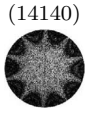 (20520)	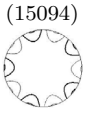 (20246)
24010	23900	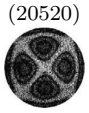 (23840)	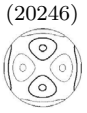 (25160)
—	—	—	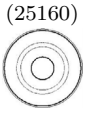 (27929)
29210	—	 (29230)	 (28531)
35210	35330	 (35280)	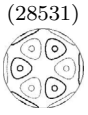 (36914)
38410	38450	 (38380)	 (37974)
—	40425	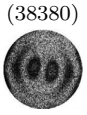 (40240)	 (42456)
—	—	—	 (48495)
48410	—	 (48310)	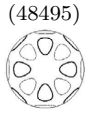 (50147)
55610	55800	 (55630)	 (58499)
57610	—	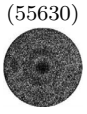 (57600)	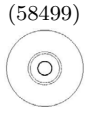 (61068)
60410	60625	 (60460)	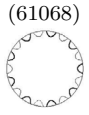 (60014)
62010	62375	 (62200)	 (64692)
—	—	—	 (72457)
72410	72500	 (72360)	 (75857)

[1]The units of the frequencies are hertz.

sented for out-of-plane and in-plane vibrations. A full-field optical method based on the AF-ESPI technique with good fringe visibility and noise reduction has been used to obtain the resonant frequencies and the corresponding mode shapes of piezoceramic circular disks with various electrode designs. The resonant frequencies of piezoceramic disks also are determined by impedance analysis, LDV, and FEM to compare with the result obtained by AF-ESPI. We find that, for the first eight out-of-plane modes, the mode shapes and resonant frequencies are almost the same for different electrode design. But for the in-plane modes, the number of modes that can be excited and the resonant frequencies are strongly influenced by electrode designs. When the impedance analysis is applied to analyze the resonant frequencies, the in-plane modes and some of the out-of-plane modes can be identified in the impedance variation curve. The full-field mode shapes obtained at resonant frequencies by using the AF-ESPI method, together with the results of finite-element calculation, impedance analysis, and LDV can provide the complete information of the vibration characteristics of piezoceramic disks with different electrode designs.

REFERENCES

[1] W. P. Mason, *Piezoelectric Crystals and Their Application to Ultrasonics*. New York: Van Norstrand, 1950.

[2] C. K. Lee, W. W. Chiang, and T. C. O'Sullivan, "Piezoelectric modal sensors/actuators pair for critical active damping vibration control," *J. Acoust. Soc. Amer.*, vol. 90, no. 1, pp. 374–384, 1991.
[3] N. Kharouf and P. R. Heyliger, "Axisymmetric free vibration of homogeneous and laminated piezoelectric cylinders," *J. Sound Vib.*, vol. 174, no. 4, pp. 539–561, 1994.
[4] H. A. Kunkel, S. Locke, and B. Pikeroen, "Finite-element analysis of vibrational modes in piezoelectric ceramics disks," *IEEE Trans. Ultrason., Ferroelect., Freq. Contr.*, vol. 37, no. 4, pp. 316–328, 1990.
[5] N. Guo, P. Cawley, and D. Hitchings, "The finite element analysis of the vibration characteristics of piezoelectric disks," *J. Sound Vib.*, vol. 159, no. 1, pp. 115–138, 1992.
[6] E. A. G. Shaw, "On the resonant vibrations of thick barium titanate disks," *J. Acoust. Soc. Amer.*, vol. 28, no. 1, pp. 38–50, 1956.
[7] G. H. Schmidt, "Extensional vibrations of piezoelectric plates," *J. Eng. Math.*, vol. 6, no. 2, pp. 133–142, 1972.
[8] D. B. Bogy and D. K. K. Miu, "Transient voltage across axisymmetrically loaded piezoelectric disks with electrodes faces," *J. Acoust. Soc. Amer.*, vol. 71, no. 2, pp. 487–497, 1982.
[9] D. B. Bogy and S. E. Bechtel, "Electromechanical analysis of nonaxisymmetrically loaded piezoelectric disks with electrodes faces," *J. Acoust. Soc. Amer.*, vol. 72, no. 5, pp. 1498–1507, 1982.
[10] C. H. Huang and C. C. Ma, "Experimental and numerical investigations of resonant vibration characteristics for piezoelectric plates," *J. Acoust. Soc. Amer.*, vol. 109, no. 6, pp. 2780–2788, 2001.
[11] N. F. Ivina, "Analysis of the natural vibrations of circular piezoceramic plates with partial electrodes," *Acoust. Phys.*, vol. 47, no. 6, pp. 714–720, 2001.
[12] I. Ohno, "Rectangular parallelepiped resonance method for piezoelectric crystals and elastic constants of alpha-quartz," *Phys. Chem. Miner.*, vol. 17, no. 5, pp. 371–378, 1990.
[13] H. Ogi, Y. Kawasaki, M. Hirao, and H. Ledbetter, "Acoustic spectroscopy of lithium niobate: elastic and piezoelectric coefficients," *J. Appl. Phys.*, vol. 92, no. 5, pp. 2451–2456, 2002.
[14] J. N. Butters and J. A. Leendertz, "Speckle patterns and holographic techniques in engineering metrology," *Opt. Laser Techn.*, vol. 3, no. 1, pp. 26–30, 1971.
[15] S. Nakadate, H. Saito, and T. Nakajima, "Vibration measurement using phase-shifting stroboscopic holographic interferometry," *Opt. Acta*, vol. 33, no. 10, pp. 1295–1309, 1986.
[16] R. Jones and C. Wykes, *Holographic and Speckle Interferometry*. Cambridge, England: Cambridge Univ. Press, 1989.
[17] M. C. Shellabear and J. R. Tyrer, "Application of ESPI to three-dimensional vibration measurements," *Opt. Lasers Eng.*, vol. 15, pp. 43–56, 1991.
[18] G. Graham, J. Petzing, M. Lucas, and J. Tyrer, "Quantitative modal analysis using electronic speckle pattern interferometry," *Opt. Lasers Eng.*, vol. 37, no. 2, pp. 147–161, 1999.
[19] W. C. Wang, C. H. Hwang, and S. Y. Lin, "Vibration measurement by the time-averaging electronic speckle pattern interferometry method," *Appl. Opt.*, vol. 35, no. 22, pp. 4502–4509, 1996.
[20] C. H. Huang and C. C. Ma, "Vibration characteristics for piezoelectric cylinders using amplitude-fluctuation electronic speckle pattern interferometry," *AIAA J.*, vol. 36, no. 12, pp. 2262–2268, 1998.
[21] C. C. Ma and C. H. Huang, "The investigation of three-dimensional vibration for piezoelectric rectangular parallel pipes using the AF-ESPI method," *IEEE Trans. Ultrason., Ferroelect., Freq. Contr.*, vol. 48, no. 1, pp. 142–153, 2001.
[22] C. K. Lee and G. Y. Wu, "High performance Doppler interferometer for advanced optical storage system," *Jpn. J. Appl. Phys.*, vol. 38, no. 3B, pp. 1730–1741, 1999.
[23] C. H. Huang, Y. C. Lin, and C. C. Ma, "Theoretical analysis and experimental measurement for resonant vibration of piezoceramic circular plates," *IEEE Trans. Ultrason., Ferroelect., Freq. Contr.*, to be published.

Yu-Chih Lin received the B.S. degree in mechanical engineering from the National Taiwan University, Taipei, Taiwan, Republic of China, and the M.S. degree in biomedical engineering from National Cheng Kung University, Tainan, Taiwan, Republic of China, in 1994 and 1996, respectively. She is currently a candidate for the Ph.D. degree in the Department of Mechanical Engineering, National Taiwan University, where she is engaged in research on resonant characteristics of piezoelectric disks under water.

Her research interests are in the fields of vibration analysis of piezoelectric materials and photomechanics.

Chien-Ching Ma received the B.S. degree in agriculture engineering from the National Taiwan University, Taipei, Taiwan, Republic of China, in 1978, and the M.S. and Ph.D. degrees in mechanical engineering from Brown University, Providence, RI in 1982 and 1984, respectively.

From 1984 to 1985, he worked as a postdoc in the Engineering Division, Brown University. In 1985, he joined the faculty of the Department of Mechanical Engineering, National Taiwan University, Taipei, Taiwan, Republic of China, as an associate professor. He was promoted to full professor in 1989.

His research interests are in the fields of wave propagation in solids, fracture mechanics, solid mechanics, piezoelectric material, and vibration analysis.